From the Eastern Vascular Society

A porcine model of thoracic aortic aneurysms created with a retrievable drug infusion stent graft mirrors human aneurysm pathophysiology

Dahlia M. Kenawy, MD,[a] Jordan F. Stafford, MD,[a] Foued Amari, MS,[a] Drayson Campbell, BS,[b] Mahmoud Abdel-Rasoul, MS, MPH,[c] Jennifer Leight, PhD,[d] Youngjae Chun, PhD,[e] *and* Bryan W. Tillman, MD, PhD,[a] *Columbus, OH; and Pittsburgh, PA*

ABSTRACT

Objective: Aneurysm pathophysiology remains poorly understood, in part from the disparity of murine models with human physiology and the requirement for invasive aortic exposure to apply agents used to create aneurysm models. A retrievable drug infusion stent graft (RDIS) was developed to isolate the aortic wall intraluminally for drug exposure. We hypothesized that an RDIS could deliver aneurysm-promoting enzymes to create a porcine model of thoracic aneurysms without major surgical exposure.

Methods: Retrievable nitinol stent graft frames were designed with an isolated drug delivery chamber, covered with polytetrafluoroethylene, and connected to a delivery wire with a drug infusion catheter installed to the outer chamber. Institutional Animal Care and Use Committee-approved Yorkshire pigs (n = 5) underwent percutaneous access of the femoral artery, baseline aortogram and stent placement in the thoracic aorta followed by 30-minute exposure to a cocktail of elastase, collagenase, and trypsin. After aspiration of excess drug, stent retrieval, and femoral artery repair, animals were recovered, with angiograms at 1 and 4 weeks followed by explant. Histological analysis, in situ zymography, and multiplex cytokine assays were performed.

Results: The RDIS isolated a segment of anterior aorta angiographically, while the center lumen preserved distal perfusion during drug treatment (baseline femoral mean arterial pressure, 70 ± 14 mm Hg; after RDIS, 75 ± 12; $P = .55$). Endovascular induction of thoracic aneurysms did not require prior mechanical injury and animals revealed no evidence of toxicity. Within 1 week, significant aneurysmal growth was observed in all five animals (1.4 ± 0.1 cm baseline to 2.9 ± 0.7 cm; $P = .002$) and only within the treated region of the aorta. Aneurysms persisted out to 4 weeks. Aneurysm histology demonstrated loss of elastin and collagen that was otherwise preserved in untreated aorta. Proinflammatory cytokines and increased matrix metalloproteinase activity were increased significantly within the aneurysm.

Conclusions: An RDIS achieves isolated drug delivery while preserving distal perfusion to achieve an endovascular porcine model of thoracic aneurysms without major surgery. This model may have value for surgical training, device testing, and to better understand aneurysm pathogenesis. Most important, although the RDIS was used to simulate aortic pathology, this tool offers intriguing horizons for focused therapeutic drug delivery directly to aneurysms and, more broadly, focused locoregional drug delivery to vessels and vascular beds. (JVS—Vascular Science 2024;5:100212.)

Clinical Relevance: The pathology behind aortic aneurysms remains poorly understood owing to limitations of current animal models. A novel drug infusion stent graft was developed to create endovascular aneurysms in a porcine model without open surgery. Aortic dilation, loss of both smooth muscle cells and elastin, as well as pro-inflammatory cytokines mirror findings in human aneurysms. The additional finding of endogenous enzyme activity suggests that this may underscore the self sustaining pathology of aneurysms. This model offers a platform to understand the biology of aneurysms and the retrievable drug infusion stent offers an important tool to potentially deliver therapies to potentially treat aneurysms.

Keywords: Aneurysm model; Endovascular; Thoracic aortic aneurysm; Porcine; Retrievable stent graft

From the Division of Vascular Surgery, The Ohio State University Wexner Medical Center, Columbus[a]; the College of Medicine,[b] Department of Biomedical Informatics,[c] and Department of Biomedical Engineering,[d] The Ohio State University, Columbus; and the Swanson School of Engineering, University of Pittsburgh, Pittsburgh.[e]

This study was supported by the National Institute of Biomedical Imaging and Bioengineering of the National Institutes of Health under award number R01EB022591 (BT and YC). DMK and JFS were supported by the National Institutes of Health under the Ruth L. Kirschstein National Research Service Award, from the National Institute of Allergy and Infectious Diseases of the National Institutes of Health under Award Number NIH T32AI106704. The content is solely the responsibility of the authors and does not necessarily represent the official views the National Institutes of Health.

Presented at the 2023 Eastern Vascular Society Meeting, Washington, DC, September 8, 2023.

Additional material for this article may be found online at www.jvsvs.org.

Correspondence: Bryan W. Tillman, MD, PhD, Division of Vascular Surgery, The Ohio State University Wexner Medical Center, 701 Prior Hall, 376 W 10th Ave, Columbus, OH 43210 (e-mail: bryan.tillman@osumc.edu).

The editors and reviewers of this article have no relevant financial relationships to disclose per the JVS-Vascular Science policy that requires reviewers to decline review of any manuscript for which they may have a conflict of interest.

2666-3503

https://doi.org/10.1016/j.jvssci.2024.100212

Death from aneurysms ranks as a leading cause of death over age 65 in the United States,[1] and yet the underlying pathogenesis remains poorly understood. Although risk factors such as hypertension and connective tissue disorders have been well-known,[2-4] recent literature has demonstrated an inflammatory component also plays a role in disease progression.[5,6] Two significant barriers to further investigation include the absence of a suitable model in which to study aneurysms but also a means by which to deliver candidate study agents to the aortic wall.

Murine models are commonly referenced in the literature,[7-9] but are limited by their small size and disparate hemodynamics as compared with humans[10] Small size also limits the ability to perform device testing. Focused aneurysm development in rodents has included open surgical exposure aortic topical application or intraluminal infusion using calcium chloride or elastase[7,11-16] The angiotensin II murine infusion[17,18] was also described to generate aneurysms without surgical exposure. A limitation of the enzymatic approaches is the requirement for open surgical exposure of the aorta to provide vascular isolation for delivery of aneurysm promoting agents (enzymes or calcium chloride) that might otherwise have toxicity if delivered into the entire circulation.

In porcine models, the use of pericardial or peritoneal patches placed during an open surgery has been used to create aneurysms[19,20] and besides a requirement for open surgical exposure, each of these methods leaves behind foreign materials and are less representative of true aneurysm wall pathology (Supplementary Table). Alternately, several porcine enzymatic and chemical aneurysm models have also been reported,[21-24] with elastase, collagenase, or calcium chloride being common agents reported. As with rodent models, open surgery to apply these agents not only prolongs recovery time and increases morbidity, but also promotes adhesions that can alter normal aneurysm behavior. To date, the only true endovascular approach was detailed by Lederman et al,[21] which used tandem occlusive balloons in a porcine model to restrain the enzymes within a confined segment of aorta; however, this approach also carries several disadvantages. One of the most notable drawbacks of this and other porcine models is the requirement for aortic occlusion. Although aortic occlusion is necessary to prevent agents infused in the aortic lumen from entering the systemic circulation, this step also results in loss of distal perfusion and ischemic injury, a problem that is even more profound when aortic occlusion occurs proximally, in the thoracic aorta. A second barrier is that, because aneurysm-promoting agents are known to cause neuronal injury,[21] the aortic branches to the spinal cord had to be covered by the tandem balloons. Because the intercostal and lumbar arteries are often within only a few centimeters of each other, this factor inherently limits the length of the aorta that can be treated to become an aneurysm. Another important finding of that same study[21] was that intraluminal elastase alone did not create aneurysms effectively and may underscore the success of others in rabbit[25] and porcine[22,23] models by the use of initial intimal injury of the aorta to improve penetration of enzymes into the media and hence cause aneurysmal change.

ARTICLE HIGHLIGHTS

- **Type of Research:** Porcine model
- **Key Findings:** A retrievable drug infusion stent achieved perfusion preserving focused delivery of enzymes to the aorta causing thoracic aneurysmal growth (1.4 to 2.9 cm; $P = .002$) in five pigs by 1 week.
- **Take Home Message:** Four week aneurysms revealed loss of elastin, decreased cellularity, increased inflammatory cytokines, and increased matrix metalloproteinases, consistent with human aneurysms.

In summary, although a porcine model represents a better hemodynamic and size match to the human condition, current approaches require open surgical exposure of the abdominal or thoracic aorta, aortic clamping with distal ischemia, and limitations on aneurysm length. A method to generate aneurysms without open surgical exposure while preserving distal perfusion during drug treatment and preventing drug entry into the spinal cord perfusion would improve significantly the usefulness of the porcine aneurysm model.

To meet these challenges, we explored the use of an entirely endovascular created porcine model of descending thoracic aorta aneurysm using a retrievable drug infusion stent graft (RDIS). Our group has demonstrated previously the use of a dumbbell-shaped retrievable stent graft to compartmentalize the injured aortic wall for clamp-free suture repair of traumatic aortic injuries while maintaining distal perfusion[26] and augmented perfusion of abdominal organs.[27] For the current application of drug delivery, an outer compartment isolated from aortic flow provided the opportunity for localized drug infusion while limiting systemic toxicity (Fig 1).

A noteworthy advantage of the RDIS is that the stent graft is retrievable by simple advancement of a vascular sheath, ensuring stent graft removal after drug delivery and, furthermore, removal from the original femoral access and leaving no stent behind. A limitation of the original dumbbell design was that torus shaped outer chamber exposes the inner aortic wall to 360° drug exposure and does not effectively exclude entry of neurotoxic agents into posteriorly located lumbar and intercostal branches to the spinal cord. For this reason, the RDIS was modified to move the center lumen eccentrically posterior such that the center lumen itself covers the branches to the spinal cord. A final challenge was the need to disrupt the protective intimal layer to allow entry

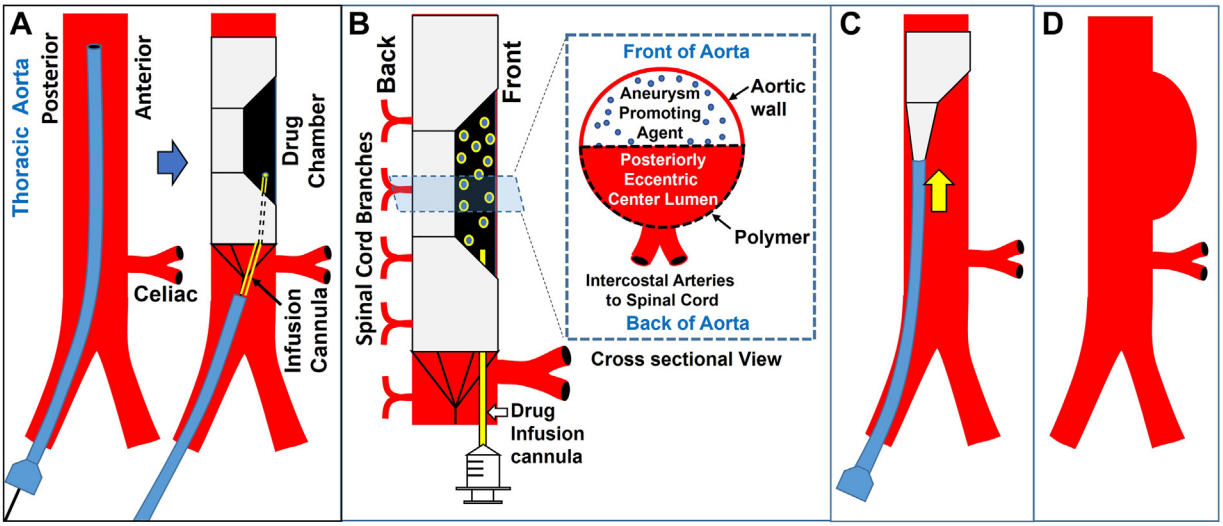

Fig 1. Strategy for an endovascular created thoracic aortic aneurysm. **(A)** After delivery of a retrievable drug infusion stent graft (RDIS), the stent is deployed by sheath withdrawal. **(B)** An aneurysm promoting drug is infused through a cannula into the drug chamber facing the anterior aortic wall, while the posteriorly place center lumen effectively occludes flow into the branches perfusing the spinal cord (inset). **(C)** After drug treatment, the RDIS is recovered by sheath advancement to collapse the stent and **(D)** an aneurysm should develop over days to weeks.

of aneurysm-promoting enzymes into the aortic wall. Although other investigators reported success with pressure-induced mechanical injury,[25] our experience revealed that balloon angioplasty consistently caused intimal injury of the posterior wall, which is opposite the side from the intended enzyme infusion (Supplementary Fig). As an alternative, this study explored trypsin, widely used in cell culture and tissue decellularization protocols,[28,29] to remove the endothelium and facilitate aortic wall drug entry without the need for mechanical injury.

We hypothesized that this newly designed RDIS could be used to develop an entirely endovascular descending thoracic aortic aneurysm porcine model while maintaining distal perfusion and excluding entry into the spinal perfusion during enzyme instillation to the aortic wall. We further hypothesized that this approach would avoid the need for initial mechanical injury of the intima.

METHODS

RDIS development

Methodology for retrievable stent grafts has been described previously.[26,30] Briefly, self-expanding nitinol scaffolds (Confluent Medical, Scottsdale, AZ) were laser-cut based on custom stent designs with SolidWorks (Dassault Systèmes SolidWorks Corporation, Waltham, MA). Next, scaffolds were thermally shapeset using a customized mandrel imparting an eccentrically oriented center lumen. Stent scaffolds were then covered with electrospun polytetrafluoroethylene (Bioweb, Zeus, Orangeburg, SC). The proximal and distal diameters of the stent graft measured 27 mm and the mid-zone measured 12 mm on anterior-posterior dimension, with a total length of 28 cm. The length of the outer drug delivery chamber was 12 cm. The distal end of the stent grafts was permanently affixed to a stiff delivery wire (Lunderquist, Cook Medical, Bloomington, IN) to facilitate deployment and recapture. The tip of an 0.018-inch catheter (Quick-Cross, Koninklijke Philips NV, Amsterdam, the Netherlands) was positioned alongside the delivery wire and then through the polytetrafluoroethylene into the drug delivery chamber of the stent graft. At the opposite end of the catheter the injection hub extended through the femoral access to facilitate both drug infusion and aspiration from outside the body. The completed stent grafts were sterilized and collapsed within a 12F vascular sheath (Cook Medical) for in vivo deployment. The completed RDIS is illustrated in Fig 2, *A-E*.

An endovascular created porcine thoracic aneurysm model

Animals studies were conducted in accordance with NIH guidelines and the protocol was approved by The Ohio State University Institutional Animal Care and Use Committee (#2020A00000088) and followed the ARRIVE Guidelines. Five Yorkshire cross pigs (1 female, 4 males; 74 .0 ± 3.9 kg) were sedated with Tiletamine 300 mg intramuscular (IM) once and placed under general endotracheal anesthesia with isoflurane 2% to 5% until recovery. Percutaneous right femoral arterial access was obtained and upsized to a primary 16F sheath (Cook Medical) (Fig 2, *F*), which was used to obtain baseline arterial pressures and used as an entry for delivery of a secondary sheathed RDIS into the aorta. Animals were

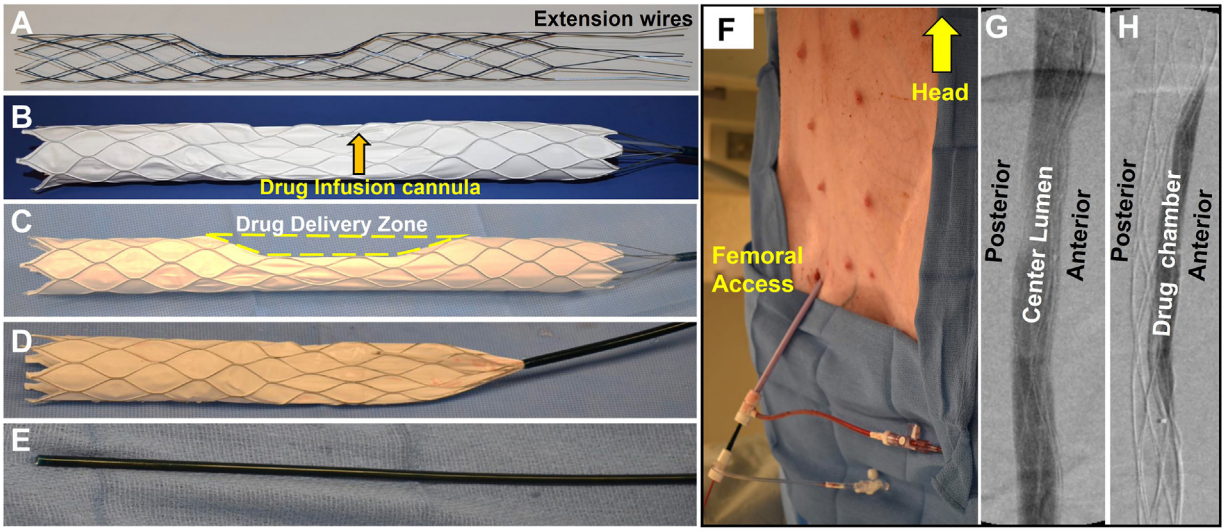

Fig 2. Retrievable drug infusion stent graft RDIS). **(A)** Bare shapeset nitinol scaffold. Front **(B)** and side **(C)** views of the RDIS depicting the drug infusion cannula and drug delivery zone. **(D)** RDIS being recaptured within a 12F sheath and **(E)** after complete recapture. **(F)** Percutaneous access of the femoral artery. Lateral angiography depicting distal flow through the center lumen **(G)** and **(H)** isolated drug infusion chamber.

heparinized at a dose of 100 U/kg as part of the standard protocol during endovascular procedures. Baseline angiography provided baseline aortic measurements and location of the celiac artery. The RDIS was then deployed under fluoroscopic guidance in the descending thoracic aorta above the celiac artery by sheath withdrawal with special attention to orient the outer chamber anteriorly. Angiography was used to document aortic flow of the center lumen and anterior chamber, and distal arterial pressure monitoring was transduced from the femoral access before and after RDIS deployment. An enzyme cocktail at an average temperature of 32°C consisted of 2.5% trypsin-EDTA (Ref 25200-056, Gibco, Thermo Fisher Scientific, Waltham, MA), 500 U elastase (Cat# LS002294, Worthington Biochemical Corporation, Lakewood, NJ), and 8000 U collagenase type 1 (Cat# LS004196, Worthington Biochemical Corporation) was instilled through the infusion lumen to the outer chamber for 30 minutes, followed by aspiration and completion angiography. The RDIS was retrieved using sheath advancement to collapse the stent. After removal of the sheath, the femoral artery was repaired with polypropylene suture through a small 3-cm femoral cutdown. Total duration of procedures from completion of anesthesia to emergence from anesthesia was under 1.5 hours. Postoperatively animals received flunixin meglumine (Banamine) 2.2 mg/kg IM every 8 hours and 0.1 mg/kg IM buprenorphine every 8 hours for breakthrough pain for the first 2 postoperative days. Animals were assessed twice daily for 2 days and then daily thereafter.

Postoperative imaging. At 1 week and 4 to 5 weeks after the initial surgery, angiograms were performed via percutaneous femoral access as a metric for aneurysm size and rate of growth. These animals received tiletamine 300 mg IM once and placed under mask anesthesia with isoflurane 2% to 5% until recovery.

End of study and explant. At 4 to 5 weeks, animals received tiletamine 300 mg IM once and anesthesia with isoflurane 2% to 5% for terminal angiogram. Representative animals underwent intravascular ultrasound examination (n = ; Volcano S5, Koninklijke Philips NV) to evaluate diameters of the (1) upper untreated thoracic aorta, (2) treated mid-thoracic aorta, and (3) lower untreated thoracic aorta. Select animals (n = 2) also underwent magnetic resonance angiography (MRA) performed on a Siemens Vida scanner (Siemens, Munich, Germany); MRA contrast was ferumoxytol 2 mg/kg diluted in 1 L saline, administered over 60 minutes intravenously. Specific parameters included 3 Tesla field strength, 400 × 322 × 120 mm field of view, 288 × 248 × 96 acquisition matri×, 0.7 x 0.7 mm spatial resolution, 511 Hz/pixel bandwidth, 2 parallel imaging acceleration rate, and a 20° flip angle). While still under isoflurane anesthesia, animals were exsanguinated until cessation of cardiac activity, followed by aortic explant from the deceased animal. Ring specimens from the untreated upper thoracic aorta, the treated mid descending, and shoulder between these two regions were preserved in formalin, zinc-based fixative for matrix metalloproteinase (MMP) histology, and or flash frozen cytokine analysis, respectively. Specimens were collected using the following naming convention: upper (normal untreated) aorta, top shoulder of aneurysm, and mid-aneurysm (Fig 3).

Histological analysis. Formalin-fixed paraffin embedded specimens were stained with either hematoxylin and eosin or Movats's pentachrome stain and evaluated using an Ni-E microscope (Nikon Inc, Melville,

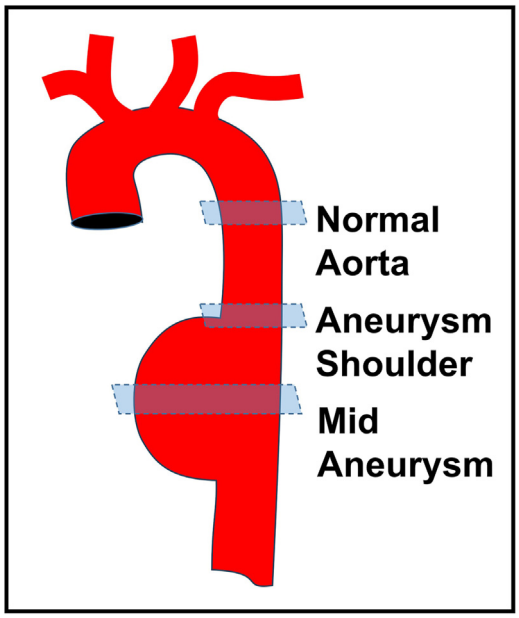

Fig 3. Sectioning diagram of the explanted aorta.

NY) to evaluate histology, thickness, and integrity of elastin/collagen within aortic specimens. Analysis was performed by Nikon Elements Basic Research Imaging Software (Nikon).

Elastin quantitation. Movat-stained histological sections, imaged at 10× magnification, had four representative sampling quadrants from each of the three groups (mid-aneurysm anterior, mid-aneurysm posterior, normal thoracic aorta). As previously described,[31] the total media area was measured first as the total area bound between the internal and external elastic laminae using Nikon NIS-Elements imaging software. The total elastin area within the media was calculated using a standardized binary threshold mask to isolate total area of elastin fibers only. Finally, the elastin area fraction was calculated as the total elastin area divided by the total media area to determine the percentage of media that is made up of elastin.

In situ zymography. In situ zymography uses a precursor fluorophore, activated through cleavage by tissue matrix MMP, to highlight the spatial location of enzyme activity within aortic specimens. Specimens were fixed in zinc-based fixative for 24 hours before paraffin embedding. In situ zymography of paraffin-embedded specimens was performed using a modified protocol by Hadler-Olsen et al.[32] Briefly, specimens were cut onto slides and deparaffinized in xylene and decreasing concentrations of ethanol, then sodium chloride and phosphate-buffered saline. Dye-quenched fluorescein conjugated gelatin (Invitrogen D12054, Thermo Fisher Scientific, Eugene, OR) was diluted 1:50 in reaction buffer and added to each specimen, which were then incubated for 2 hours at 37°C. Two additional controls were used for each specimen: MMP inhibitor (phenanthroline) and no substrate. Specimens were then imaged with a binary threshold mask laid over the fluorescence image to measure the mean intensity of only the tissue section, excluding the slide background. The mean intensity of the masked image is a unitless measure in a given area based on the ratio of photons converted to electrons at the given excitation wavelength using a Nikon Ni-E microscope and fluorescent intensity was quantified by Elements Basic Research Imaging Software (Nikon).

Multiplex analysis. A Porcine Luminex Discovery Assay (Catalog #LXSAPM, R&D Systems, Bio-Techne, Minneapolis, MN) was purchased for multiplex analysis of the following cytokines: interferon-γ, interleukin (IL)-1 alpha, IL-1 RA, IL-1 beta, IL-2, IL-4, IL-6, IL-10, IL-12, IL-18, and MMP-1. Samples for upper thoracic aorta, top shoulder of aneurysm, and mid-aneurysm were run in triplicate for each pig. In brief, frozen tissues were thawed and homogenized in 1× phosphate-buffered saline at a concentration of 100 μg/mL. Samples were centrifuged (Sorvall Legend XTR, Thermo Fisher Scientific) at 16,000×*g* for 4 minutes, then underwent 2-fold dilution. Samples were then prepared based on the multiplex manufacturer's instructions.

Statistical analysis. Sample sizes were based on an 80% power calculation to detect statistically significant differences in aortic diameters from baseline. Linear mixed effect models with random intercepts accounting for repeated measures within animals were used to estimate and test differences in outcome measurements between treatments, locations, or across time points where relevant. Results are reported as means (standard deviation). Hypothesis testing was conducted at an overall 5% type I error rate (alpha = 0.05) using the Tukey-Kramer method to adjust for multiple comparisons. SAS version 9.4 (SAS Institute, Cary, NC) was used to conduct all statistical analyses.

RESULTS

Aneurysm induction. Five Yorkshire swine underwent aneurysm induction using the RDIS delivered from a percutaneous femoral approach. Baseline aortic diameters from angiograms were 1.4 ± 0.1 cm in anteroposterior (AP) view and 1.4 ± 0.1 cm in lateral view. Stent grafts were positioned fluoroscopically in the descending thoracic aorta, with the distal end above the celiac artery. After RDIS deployment, angiograms further demonstrated preserved flow through the center lumen, and the outer chamber was isolated fluidically from the circulation (Fig 2, *G* and *H*). Distal perfusion through the stent was further confirmed in that femoral mean arterial pressures averaged 75 ± 12 mm Hg ($P = .55$) were comparable with baseline pressures averaging 70 ± 14 mm Hg averaged for all five animals. An enzyme cocktail of elastase, collagenase, and trypsin was infused from a catheter port outside the animal and after

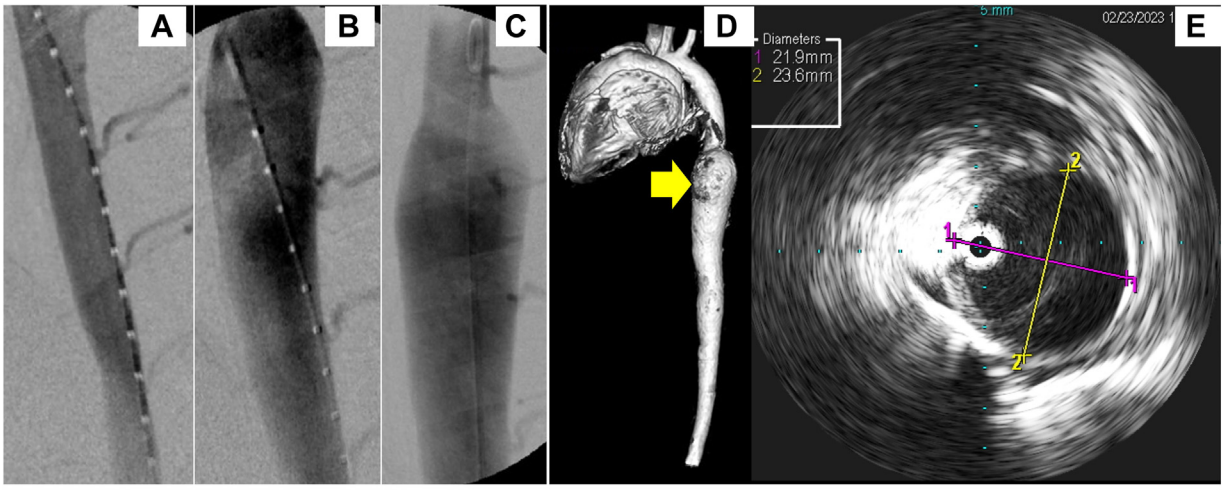

Fig 4. Representative angiogram at **(A)** baseline, **(B)** 1 week, and **(C)** 4 weeks. Representative **(D)** magnetic resonance angiography (MRA) 4 weeks and **(E)** intravascular ultrasound images (4 weeks) are also shown. Scale bars are shown in centimeters and millimeters.

minutes of aneurysm induction, the remaining enzymatic cocktail was aspirated. Angiography revealed no significant aneurysmal change from baseline, and the RDIS was recaptured by sheath advancement with suture repair of the femoral artery. Animals recovered with no evidence of neurological deficits and were ambulating by the following day.

Aneurysm assessment. A comparison of representative imaging timepoints (angiogram, MRA, and intravascular ultrasound examination) are shown in Fig 4, and 4-week angiograms and operative images for each animal are depicted in Fig 5. Aortic diameters reflect the largest aortic size in centimeters for all five study animals. At 1 week after aneurysm induction, aortic diameters angiographically measured 2.9 ± 0.7 (AP; $P = .002$ compared with baseline) and 2.8 ± 0.8 (lateral; $P = .02$ compared with baseline) (Table I). At the next study end point of 4 to 5 weeks, the AP diameter measured 2.7 ± 0.7 cm ($P = .017$ vs baseline; $P = .872$ vs 1 week) and lateral diameter measured 2.5 ± 0.8 cm ($P = .046$ vs baseline; $P = .829$ vs 1 week). Aneurysm length at 4 weeks averaged 9.2 ± 1.3 cm, which is consistent with the length of the drug delivery chamber. Imaging demonstrated bilobed aneurysm morphology consistently, which was believed to be due to external compression from the diaphragmatic crus in this location.

Explant findings. Explantation of the thoracic aorta revealed normal architecture in the untreated proximal aorta yet significant aneurysmal change in the RDIS treated aorta. Although hyperemia was observed over the aneurysm sac, no aortic perforations or erosions into adjacent organs were observed. As noted on angiograms, the caliper aneurysm length remained within the dimensions of the RDIS outer chamber.

Histology. Histology (n = 5) revealed aneurysmal change of the anterior wall with decreased cellularity on hematoxylin and eosin staining (Fig 6), and the posterior wall retained a normal appearance of the baseline vessel. Movat staining revealed a paucity of elastin and collagen confined again to the treated anterior wall (Fig 7). When elastin content was compared, the mid-aneurysm anterior wall was only 18.57% ± 9% (average ± SD), whereas untreated mid-aneurysm posterior wall was 55.0% ± 12.58% and normal untreated thoracic aorta was 58.36% ± 8.28%, with a statistically significant difference between mid-aneurysm anterior and either mid aneurysm-posterior ($P < .001$) or normal thoracic aorta ($P < .001$). In summary, loss of elastin staining corresponded with the areas of greatest aneurysmal change.

In situ zymography. When stained with a fluorescently labeled and MMP-activated precursor, MMP activity was increased significantly in the aneurysm as compared with untreated aorta (Fig 8). Comparing the whole aortic ring for fluorescent intensity for five animals, we obtained the following results: buffer control 466 ± 66 or MMP-blocked control 416 ± 41, the intensity of control untreated adjacent normal aorta with fluorescein gelatin was 711 ± 117. As compared with MMP-blocked control of untreated aorta, the mid aneurysm was significantly higher at 1307 ± 307 ($P = .0055$). Looking specifically at the anterior vs the posterior wall in the normal thoracic aorta, the values were similar and nonsignificant between anterior wall at 734 ± 121 vs posterior wall 688 ±

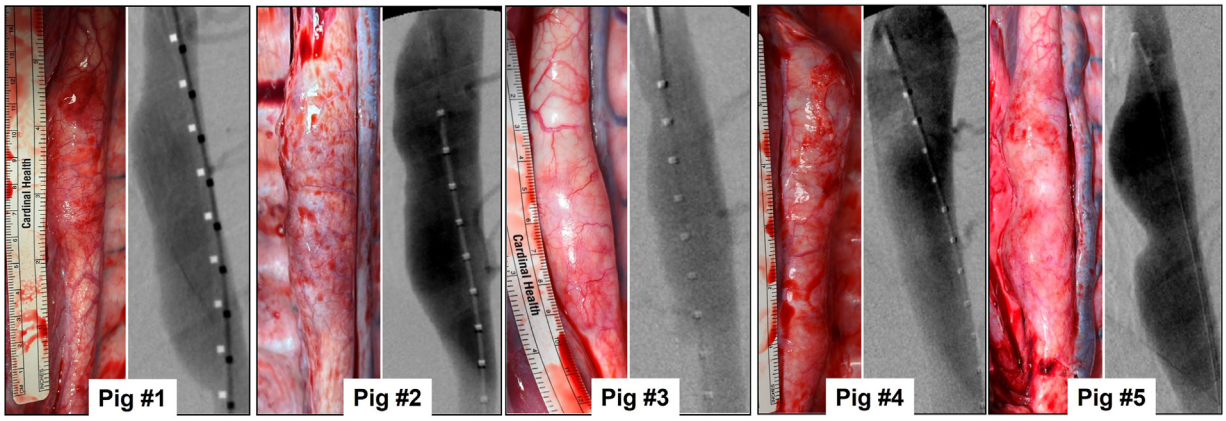

Fig 5. Explant images of five aneurysm animals at 4 weeks revealing the explant operative image and matching aortogram from the same date.

Table I. Aortic measurements in centimeters (cm) at baseline, 1 and 4 weeks

Aortic dimensions, cm	Pig 1	Pig 2	Pig 3	Pig 4	Pig 5	Average	Standard deviation
Baseline diameter (AP)	1.5	1.5	1.5	1.2	1.5	1.44	0.13
Baseline diameter (LAT)	1.6	1.4	1.3	1.4	1.3	1.4	0.12
1-Week diameter (AP)	2.5	2.6	2	3.6	3.6	2.86	0.71
1-Week diameter (LAT)	2.1	2.3	2	3.7	3.6	2.74	0.84
1-Week longitudinal length	6.4	10.3	7.9	10.9	9.6	9.02	1.85
4-Week diameter (AP)	2.4	2.2	2.5	3.4	3	2.7	0.49
4-Week diameter (LAT)	2	2	2	3.6	2.9	2.5	0.73
4-Week longitudinal length	7.1	9.1	9.8	10.6	9.6	9.24	1.31

AP, Anteroposterior; *Lat*, lateral.

131. Conversely, in the mid aneurysm, the in situ zymography signal was significantly greater in the treated anterior wall at 1621 ± 413 as compared with the untreated posterior wall 992 ± 251 ($P < .0032$).

Cytokine expression. Aortic wall specimens from all five study animals were assayed for expression of cytokines with a multiplex assay. We compared three regions of the aorta: untreated and treated aorta, as well as the intervening shoulder region of the aneurysm, testing each specimen with three technical replicates. The anterior aneurysm wall revealed elevated IL1-RA, IL-1α, IL-12, IL-18, and MMP-1 as compared with untreated thoracic aorta (Table II). It is notable that, among cytokines that were statistically significant, and with the sole exception of IL-1α, the aneurysm shoulder demonstrated values midway between untreated and aneurysmal aorta, consistent with being a transitional area between normal and aneurysmal aorta.

DISCUSSION

Our study demonstrates the feasibility and reproducibility of an endovascularly created and, at the same time, perfusion-preserving approach to creating aneurysms in the thoracic aorta of a porcine model. Although a previous study by Lederman et al[21] had reported the use of tandem endovascular occlusion balloons, that report detailed instead the abdominal aorta, incurred loss of distal aortic flow, and yielded extremely limited aneurysm length owing to the need to place occlusion balloons over immediately adjacent levels of spinal cord branches. The RDIS of this study provided several unique advantages for a large animal aneurysm model. First, the retrievable design challenges traditional tenets of a permanent stent graft in that it achieves a therapeutic (or research) task and yet was easy to remove after use to avoid the confounders of a retained foreign body. Second, the outer drug treatment chamber of the RDIS is oriented anteriorly, which matches the region of aorta most commonly affected by aneurysmal degeneration in the human condition.[33,34] Third, the posteriorly eccentric center lumen provides a baffle against the posterior aorta, effectively excluding spinal perfusion from the potentially toxic enzymatic cocktail, allowing the creation of longer aneurysms over the tandem balloon approach. Although spinal perfusion is important, in

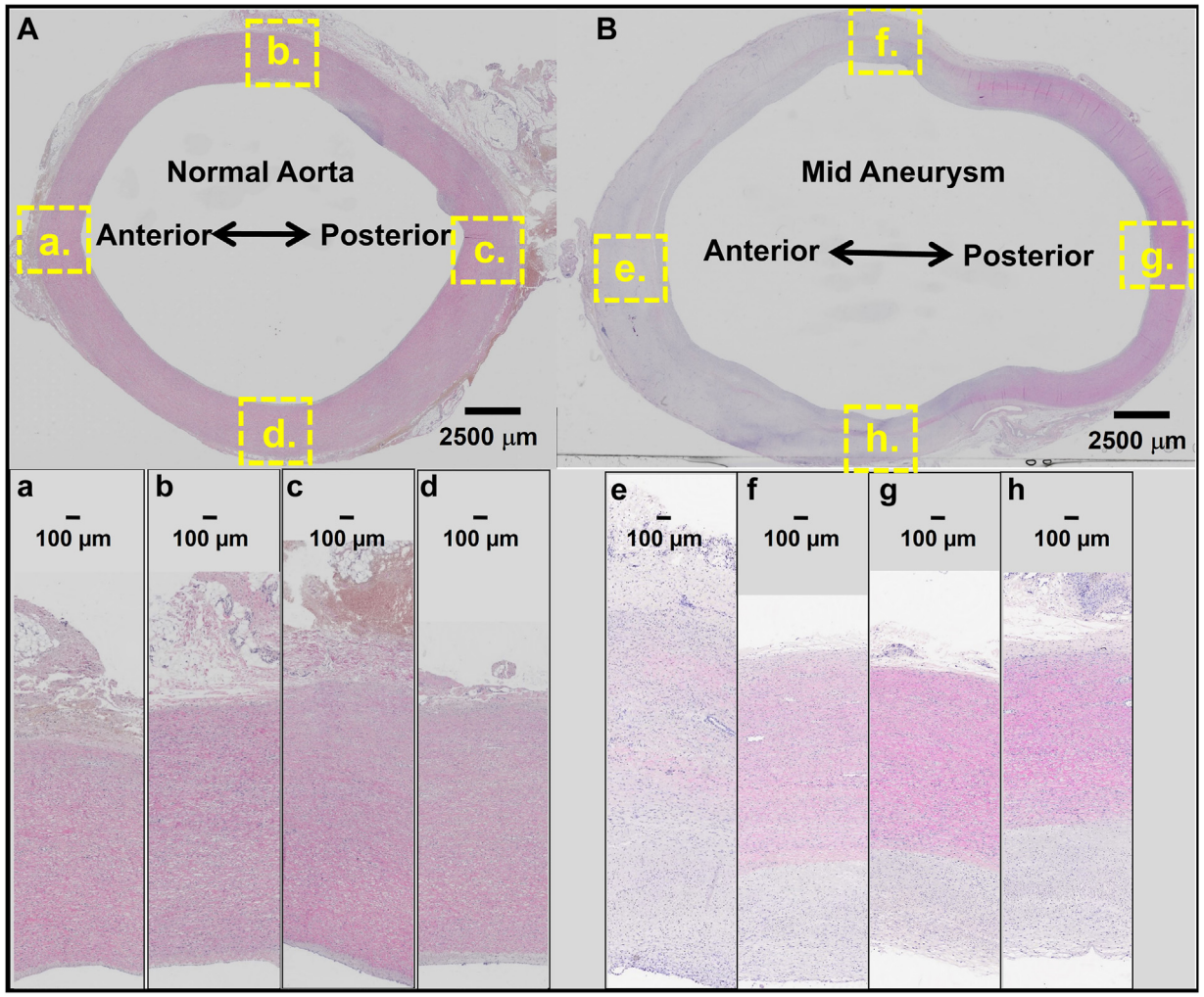

Fig 6. Compared with normal aorta **(A)** hematoxylin and eosin-stained sections from mid aneurysm **(B)** revealed decreased cellularity and connective tissue. Aneurysmal change is especially prominent in the anterior aortic wall where enzyme exposure occurred. Inset images **(A–H)** reveal magnified images (10×) from quadrants of aortic specimens.

fact, during both human open and permanent stent graft aortic repairs, multiple levels of spinal cord branches are permanently occluded rarely with any consequence, except of course when excessive lengths of aorta are repaired, such as extensive thoracoabdominal repair.[35,36] The interconnection between levels also prevents spinal cord ischemia and most importantly the period of exclusion in this model (30 minutes) is extremely brief. More objectively, in this study we observed no cases of paresis in any animals after temporary coverage of spinal perfusion with the RDIS.

Drug confinement. The confinement of a delivered drug to the outer chamber in this study was confirmed in several ways. Contrast infused in the outer chamber was confined angiographically, and aneurysmal change and deterioration of elastin and collagen layers was limited to the anterior wall facing the outer chamber. Finally, the longitudinal length of the resulting aneurysm was consistently within the length of the drug delivery chamber (<12 cm) confirming that the drug remains constrained within the anterior chamber and further evidenced by the loss of elastin content in anterior, but not the posterior wall.

Advantages of a strictly enzymatic injury. An important consideration of aneurysm models is the mechanism by which to penetrate aneurysm-generating enzymes into the medial layer of the aorta. Intraluminal infusion models have reported a requirement for prior mechanical injury (eg, balloon angioplasty) on the basis that enzyme transit into the aortic wall would be otherwise impaired.[21-23,25] Our own experience revealed that balloon angioplasty injury occurs primarily in the posterior aorta (Supplementary Fig), which is not where aneurysms usually develop and, in this model, is exactly

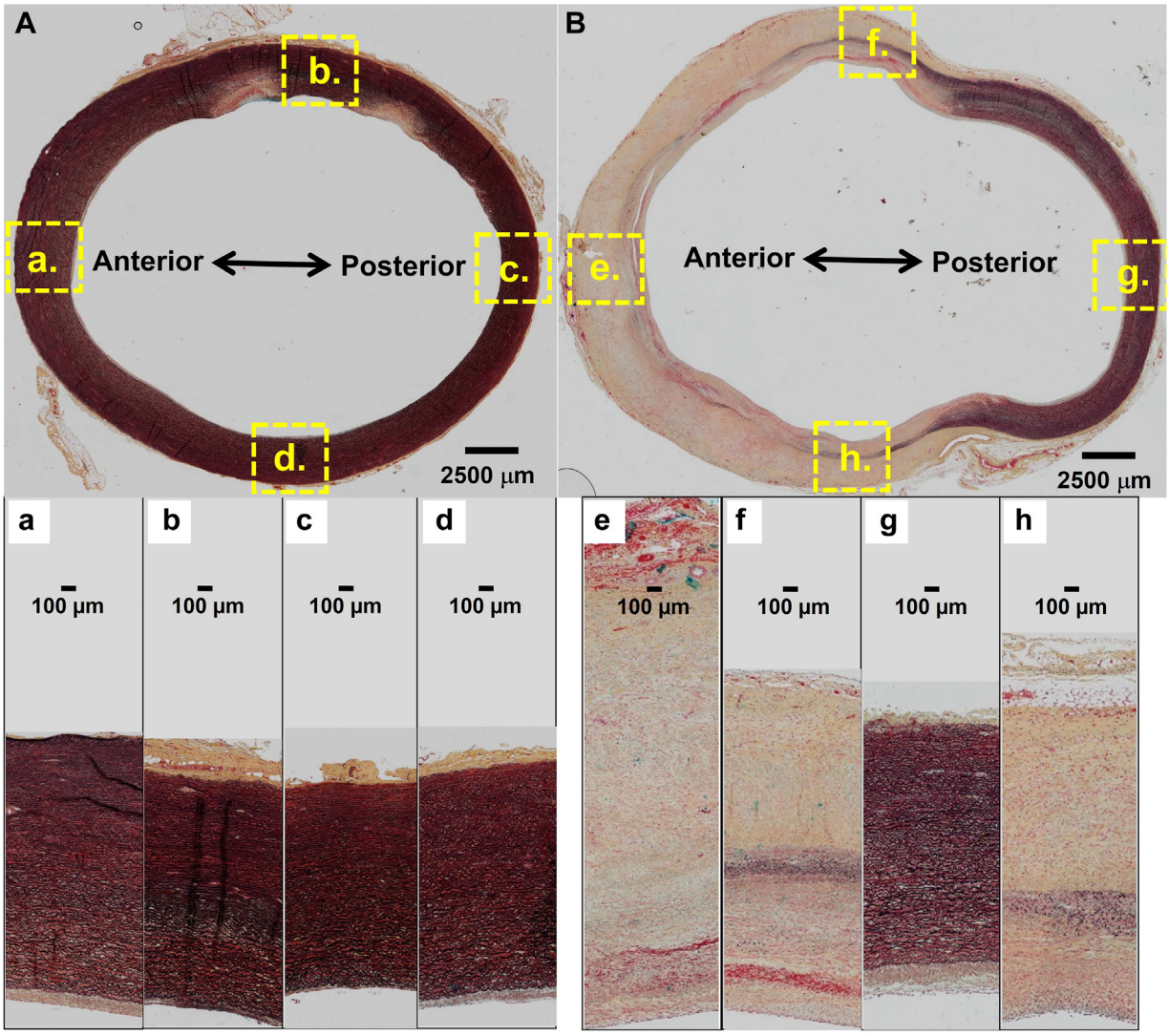

Fig 7. Movat staining of the explanted aorta. Compared with a normal distribution of elastin in normal aorta **(A)** hematoxylin and eosin-stained sections from mid aneurysm **(B)** revealed decreased elastin mirroring aneurysmal change, with preserved posterior elastin content. Inset images **(A–H)** reveal magnified images (10×) from quadrants of the aortic specimens.

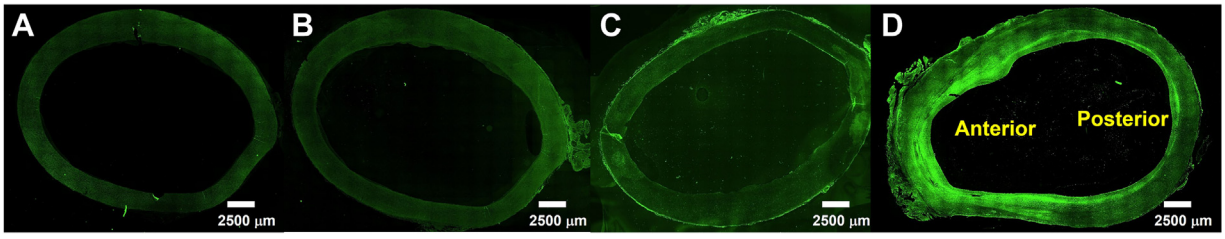

Fig 8. In situ zymography for aortic matrix metalloproteinase (MMP) activity. As compared with a buffer only control **(A)** and a control with an MMP inhibitor **(B)**, untreated thoracic aorta adjacent to the aneurysm reveals minimal edge signal **(C)**. Conversely intense MMP signal is observed in the aneurysm, particularly in the aneurysmal anterior wall **(D)**.

opposite where the enzyme is actually delivered. As an alternative, trypsin, widely used for both release of cultured endothelium[28] and even decellularization of cardiovascular specimens,[29] was used. Combined with elastase and collagenase, trypsin allowed for a pure enzymatic model without the need for mechanical

Table II. Cytokine concentrations in normal thoracic, shoulder region, and mid-aneurysm

Cytokine pg/mg	IL-1 RA	IL-1α	IL-1β	IL-2	IL-4
Normal aorta	2.5121 ± 0.3033	0.7343 ± 0.2842	0.1636 ± 0.0320	1.3773 ± 0.3069	11.5760 ± 0.8017
Top shoulder	2.9630 ± 0.3033	0.6298 ± 0.2759	0.1848 ± 0.0305	1.1368 ± 0.3000	9.7428 ± 0.7786
Mid-aneurysm	5.1287 ± 0.3033	1.7224 ± 0.2303	0.2349 ± 0.0287	1.1940 ± 0.2946	10.5564 ± 0.7420
P value	**<.0001**	**.0070**	.1087	.5134	.3967

IFN, Interferon; *IL,* interleukin; *MMP,* matrix metalloproteinase.
Values are average ± standard error.
Bold values depicts statistical significance.

injury. This development is important because enzymatic treatment alone is likely to yield a more consistent injury of the aortic wall as compared with the focal mechanical injury of other approaches. Importantly for this proof-of-concept study, we used a cocktail of enzymes, whereas single-agent enzyme merits further investigation and may yield similar results. Enzymes are exquisitely temperature sensitive, and, for this study, enzymes were administered at an average of 32°C. Details of the optimal temperature merit further investigation.

Loss of elastin and cellularity. Loss of elastin integrity is a hallmark of human aneurysms and the loss, isolated to the anterior wall, was quite profound in this model. We expect that the downtitration of elastase or the duration of exposure in future studies may result in lesser degrees of elastin degradation. A quite notable finding was the loss of cellularity in the exposed aortic wall. Although the enzyme cocktail has no cytotoxic effects, apoptosis of smooth muscle cells as a result of elastin degradation[37] and direct cellular cytotoxicity[38] by infiltrating monocytes merits further investigation. These findings mirror the loss of vascular smooth muscle cells in human aneurysms.[39]

Persistent proinflammatory and endogenous MMP activity. By many accounts, an aneurysm is probably a smoldering pathophysiology, perpetuated by continuous cascades of insult, whether hemodynamic (hypertension), smoking, or a proinflammatory environment.[40] For this study, we reasoned that aneurysm induction may trigger longer term inflammation and intrinsic enzymatic activity. Cytokines are a key mediator of inflammatory changes and our findings suggest that several proinflammatory cytokines previously linked to aneurysm pathology are indeed elevated as far as 4 weeks after aneurysm initiation including IL-1α, IL-12, and IL-18.[8,41-45] IL-12 and IL-18 have each been reported specifically as elevated in human aneurysms.[46,47] MMP activity meanwhile has been linked to aneurysm growth[2,40,48,49] and is believed to mediate further damage of aortic connective tissue. Besides the elevation of MMP1 identified in this study with multiplex assay, we reasoned that intrinsic MMP activity more broadly may persist after an aortic aneurysm is created in this model. In situ zymography is a powerful tool in that it reveals spatially, within a tissue specimen, where the increased enzymatic activity is occurring. Our results highlight persistent MMP activity identified as far as 4 weeks after aneurysm initiation, but especially in the treated aneurysmal anterior aortic wall. It is notable that the untreated posterior wall exhibited some increase in MMP, and this finding may be related to bystander inflammation adjacent to the treated anterior wall. Further studies will be needed to determine if the increased MMP activity persists beyond 4 weeks and may help to better define whether this activity underscores long-term aneurysm growth.

Expected growth after aneurysm induction. It is notable that aneurysms developed as soon as 1 week after enzymatic initiation but remained the same cross-sectional diameter. Arguably, in humans, the natural history of aneurysm growth is slow, typically between 2.8 and 4.2 mm per year[50,51]; thus, the 4-week end point of this current study is exceedingly short by comparison. The increase in wall tension predicted by Laplace's law[52] might impart additional growth, but this factor will need to be determined experimentally with longer term studies.

Study limitations. In addition to uncertainty about long-term aneurysm growth from this proof-of-concept study, future studies will also need to explore the molecular changes, which are certain to be critical to aneurysm development. Although angiography revealed isolation of the outer chamber and we observed no clinical evidence of enzyme leakage, tracer studies will be important to quantify more objectively any systemic drug losses from the outer compartment. Furthermore, although the exposure of enzymes to the anterior wall is necessary to avoid exposure to the spinal cord, it does create an aneurysm that is more saccular than fusiform. This finding may be helpful for the study of saccular aneurysms, which are generally less predictable than fusiform aneurysms[53] Finally, although imaging reflects aortic size at several timepoints, histology and inflammatory data in this study reflect only a single timepoint. As a result, future studies will need to

Table II. Continued.

IL-6	IL-10	IL-12	IL-18	MMP-1	IFN-γ
1.0564 ± 0.2913	1.8826 ± 0.2682	1.5965 ± 0.2835	89.3175 ± 21.8496	1.4060 ± 0.1876	0.2025 ± 0.0194
0.9900 ± 0.3794	1.9196 ± 0.2682	2.1061 ± 0.2835	121.14 ± 21.8496	1.5634 ± 0.1814	0.2179 ± 0.0194
1.4802 ± 0.2946	1.7634 ± 0.2668	3.0497 ± 0.2835	306.40 ± 21.8496	1.9663 ± 0.1766	0.2518 ± 0.0198
.3334	.6866	**<.0001**	**<.0001**	**.0028**	.0599

compare these findings at both earlier and later timepoints.

CONCLUSIONS

The benefits of an RDIS aneurysm model include a small femoral exposure and endovascular drug delivery that should offer more rapid recovery, reduced ischemic time compared with crossclamp or balloon occlusion models, and avoidance of abdominal/thoracic incisions, as well as adhesions that might impact aneurysm growth and subsequent study interventions adversely. The retrievability of this stent graft after use avoids the potential confounder and risks of a permanent, implanted device. The preserved distal perfusion is particularly attractive, because it allows a longer duration of drug therapy, without ischemic injury below the treatment area. The ability to avoid spinal cord perfusion with the aneurysm-inducing cocktail and resultant chemical injury, as well as orientation of the aneurysm on the anterior wall similar to the human condition, are additional positive attributes. This model has particular usefulness in long-term studies of aneurysm progression before and after permanent aortic endografts, which are otherwise prohibitive in small murine models. Moreover, this model offers opportunities in surgical education where experience in open repair during training has become increasingly less common and yet remains an essential skillset for the vascular surgeon[54] Most important, although this study used the RDIS to deliver agents that incite aneurysmal pathology, the most exciting horizon of the approach is the opportunity to instead deliver candidate therapies to the aortic wall with a goal of stabilizing the aneurysm wall. This technology may even have broad applicability in other contexts of locoregional drug delivery, where an agent may otherwise be toxic at the systemic level but offer a higher effective dose when delivered focally at the target.

The authors thank Orlando Simonetti, PhD, of the Cardiac Imaging Research Center at The Ohio State University for supervision of magnetic resonance imaging and the Interventional Cardiology Cath Core Lab of the Ohio State University for angiography support. The authors also thank the Clinical Translational Science Shared Resource for multiplex analysis of aortic samples and the Comparative Pathology & Digital Imaging Shared Resource for histological processing, both at The Ohio State University and supported in part by a National Cancer Institute Grant (P30 CA016058).

AUTHOR CONTRIBUTIONS

Conception and design: DK, JS, YC, BT
Analysis and interpretation: DK, JS, MA, YC, BT
Data collection: DK, JS, DC, BT
Writing the article: DK, JS, FA, DC, JL, YC, BT
Critical revision of the article: DK, JS, MA, BT
Final approval of the article: DK, JS, FA, DC, MA, JL, YC, BT
Statistical analysis: MA, BT
Obtained funding: DK, JS, YC, BT
Overall responsibility: BT
DK and JS contributed equally to this article and share co-first authorship.

DISCLOSURES

B.W.T. and Y.C. have filed for intellectual property of the retrievable stent design used in this study.

REFERENCESS

1. *National Center for Injury Prevention and Control WISQARS Leading Causes of Death Reports*. Centers for Disease Control and Prevention; 2020.
2. Ruddy JM, Jones JA, Ikonomidis JS. Pathophysiology of thoracic aortic aneurysm (TAA): is it not one uniform aorta? Role of embryologic origin. *Prog Cardiovasc Dis*. 2013;56:68–73.
3. Tsamis A, Krawiec JT, Vorp DA. Elastin and collagen fibre microstructure of the human aorta in ageing and disease: a review. *J R Soc Interface*. 2013;10:20121004.
4. Guo DC, Papke CL, He R, Milewicz DM. Pathogenesis of thoracic and abdominal aortic aneurysms. *Ann N Y Acad Sci*. 2006;1085:339–352.
5. Artemiou P, Charokopos N, Rouska E, et al. C-reactive protein/interleukin-6 ratio as marker of the size of the uncomplicated thoracic aortic aneurysms. *Interact Cardiovasc Thorac Surg*. 2012;15:871–877.
6. Hawkins RB, Salmon M, Su G, et al. Mesenchymal stem cells alter MicroRNA expression and attenuate thoracic aortic aneurysm formation. *J Surg Res*. 2021;268:221–231.
7. Tyerman Z, Dahl J, Shannon A, et al. Murine surgical model of topical elastase induced descending thoracic aortic aneurysm. *J Vis Exp*. 2019. https://doi.org/10.3791/60105.
8. Johnston WF, Salmon M, Pope NH, et al. Inhibition of interleukin-1beta decreases aneurysm formation and progression in a novel model of thoracic aortic aneurysms. *Circulation*. 2014;130(11 Suppl 1):S51–S59.
9. Shimizu K, Shichiri M, Libby P, Lee RT, Mitchell RN. Th2-predominant inflammation and blockade of IFN-gamma signaling induce aneurysms in allografted aortas. *J Clin Invest*. 2004;114:300–308.
10. Jena S, Chawla S. *The Anatomy and Physiology of Laboratory Mouse. Essentials of Laboratory Animal Science: Principles and Practices*. Springer; 2021.
11. Yue J, Yin L, Shen J, Liu Z. A modified murine abdominal aortic aneurysm rupture model using elastase perfusion and angiotensin II infusion. *Ann Vasc Surg*. 2020;67:474–481.

12. Zhu JX, Tang QQ, Zhou C, Shi XC, Yi SY, Yang Y. Establishment of a new abdominal aortic aneurysm model in rats by a retroperitoneal approach. *Front Cardiovasc Med*. 2022;9:808732.
13. Lu G, Su G, Davis JP, et al. A novel chronic advanced stage abdominal aortic aneurysm murine model. *J Vasc Surg*. 2017;66:232–242 e4.
14. Anidjar S, Dobrin PB, Chejfec G, Michel JB. Experimental study of determinants of aneurysmal expansion of the abdominal aorta. *Ann Vasc Surg*. 1994;8:127–136.
15. Anidjar S, Salzmann JL, Gentric D, Lagneau P, Camilleri JP, Michel JB. Elastase-induced experimental aneurysms in rats. *Circulation*. 1990;82:973–981.
16. Bhamidipati CM, Mehta GS, Lu G, et al. Development of a novel murine model of aortic aneurysms using peri-adventitial elastase. *Surgery*. 2012;152:238–246.
17. Daugherty A, Cassis LA. Mouse models of abdominal aortic aneurysms. *Arterioscler Thromb Vasc Biol*. 2004;24:429–434.
18. Daugherty A, Manning MW, Cassis LA. Angiotensin II promotes atherosclerotic lesions and aneurysms in apolipoprotein E-deficient mice. *J Clin Invest*. 2000;105:1605–1612.
19. Maynar M, Qian Z, Hernandez J, et al. An animal model of abdominal aortic aneurysm created with peritoneal patch: technique and initial results. *Cardiovasc Intervent Radiol*. 2003;26:168–176.
20. Perini SC, Bertolucci LH, Martins APD, Franca LHG, Aveline CC, Pereira AH. Abdominal aortic aneurysm model in swine with bovine pericardium patch. *J Vasc Bras*. 2021;20:e20210080.
21. Lederman A, Saliture Neto FT, Ferreira R, et al. Endovascular model of abdominal aortic aneurysm induction in swine. *Vasc Med*. 2014;19:167–174.
22. Shannon AH, Cullen JM, Dahl JJ, et al. Porcine model of Infrarenal abdominal aortic aneurysm. *J Vis Exp*. 2019;153.
23. Cullen JM, Lu G, Shannon AH, et al. A novel swine model of abdominal aortic aneurysm. *J Vasc Surg*. 2019;70:252–260 e2.
24. Eckhouse SR, Logdon CB, Oelsen JM, et al. Reproducible porcine model of thoracic aortic aneurysm. *Circulation*. 2013;128(11 Suppl 1):S186–S193.
25. Matsushita M, Kobayashi H, Oda K, Nishikimi N, Sakurai T, Nimura Y. A rabbit model of abdominal aortic aneurysm associated with intimal thickening. *Eur Surg Res*. 1999;31:305–313.
26. Kenawy DM, Elsisy M, Abdel-Rasoul M, et al. A dumbbell rescue stent graft facilitates clamp-free repair of aortic injury in a porcine model. *JVS Vasc Sci*. 2023;4:100100.
27. Go C, Elsisy M, Frenz B, et al. A retrievable, dual-chamber stent protects against warm ischemia of donor organs in a model of donation after circulatory death. *Surgery*. 2022;171:1100–1107.
28. Brown MA, Wallace CS, Anamelechi CC, Clermont E, Reichert WM, Truskey GA. The use of mild trypsinization conditions in the detachment of endothelial cells to promote subsequent endothelialization on synthetic surfaces. *Biomaterials*. 2007;28:3928–3935.
29. Remlinger NT, Wearden PD, Gilbert TW. Procedure for decellularization of porcine heart by retrograde coronary perfusion. *J Vis Exp*. 2012:e50059.
30. Go C, Elsisy M, Chun Y, et al. A three-tier Rescue stent improves outcomes over balloon occlusion in a porcine model of noncompressible hemorrhage. *J Trauma Acute Care Surg*. 2020;89:320–328.
31. Avolio A, Jones D, Tafazzoli-Shadpour M. Quantification of alterations in structure and function of elastin in the arterial media. *Hypertension*. 1998;32:170–175.
32. Hadler-Olsen E, Kanapathippillai P, Berg E, Svineng G, Winberg JO, Uhlin-Hansen L. Gelatin in situ zymography on fixed, paraffin-embedded tissue: zinc and ethanol fixation preserve enzyme activity. *J Histochem Cytochem*. 2010;58:29–39.
33. Goergen CJ, Johnson BL, Greve JM, Taylor CA, Zarins CK. Increased anterior abdominal aortic wall motion: possible role in aneurysm pathogenesis and design of endovascular devices. *J Endovasc Ther*. 2007;14:574–584.
34. Vorp DA, Raghavan ML, Webster MW. Mechanical wall stress in abdominal aortic aneurysm: influence of diameter and asymmetry. *J Vasc Surg*. 1998;27:632–639.
35. Aucoin VJ, Eagleton MJ, Farber MA, et al. Spinal cord protection practices used during endovascular repair of complex aortic aneurysms by the U.S. Aortic Research Consortium. *J Vasc Surg*. 2021;73:323–330.
36. Marcondes GB, Cirillo-Penn NC, Tenorio ER, et al. Multicenter study to evaluate endovascular repair of extent I-III thoracoabdominal aneurysms without prophylactic cerebrospinal fluid drainage. *Ann Surg*. 2023;278:e396–e404.
37. Colonnello JS, Hance KA, Shames ML, et al. Transient exposure to elastase induces mouse aortic wall smooth muscle cell production of MCP-1 and RANTES during development of experimental aortic aneurysm. *J Vasc Surg*. 2003;38:138–146.
38. Wang Q, Ren J, Morgan S, Liu Z, Dou C, Liu B. Monocyte chemoattractant protein-1 (MCP-1) regulates macrophage cytotoxicity in abdominal aortic aneurysm. *PLoS One*. 2014;9:e92053.
39. Rowe VL, Stevens SL, Reddick TT, et al. Vascular smooth muscle cell apoptosis in aneurysmal, occlusive, and normal human aortas. *J Vasc Surg*. 2000;31:567–576.
40. Marquez-Sanchez AC, Koltsova EK. Immune and inflammatory mechanisms of abdominal aortic aneurysm. *Front Immunol*. 2022;13:989933.
41. Yan H, Hu Y, Akk A, Ye K, Bacon J, Pham CTN. Interleukin-12 and -23 blockade mitigates elastase-induced abdominal aortic aneurysm. *Sci Rep*. 2019;9:10447.
42. Suehiro C, Suzuki J, Hamaguchi M, et al. Deletion of interleukin-18 attenuates abdominal aortic aneurysm formation. *Atherosclerosis*. 2019;289:14–20.
43. Ahmad M, Kuravi S, Hodson J, et al. The Relationship between serum interleukin-1alpha and asymptomatic infrarenal abdominal aortic aneurysm size, morphology, and growth rates. *Eur J Vasc Endovasc Surg*. 2018;56:130–135.
44. Tang PC, Yakimov AO, Teesdale MA, et al. Transmural inflammation by interferon-gamma-producing T cells correlates with outward vascular remodeling and intimal expansion of ascending thoracic aortic aneurysms. *FASEB J*. 2005;19:1528–1530.
45. Zhang L, Liao MF, Tian L, et al. Overexpression of interleukin-1beta and interferon-gamma in type I thoracic aortic dissections and ascending thoracic aortic aneurysms: possible correlation with matrix metalloproteinase-9 expression and apoptosis of aortic media cells. *Eur J Cardio Thorac Surg*. 2011;40:17–22.
46. Puchenkova OA, Soldatov VO, Belykh AE, et al. Cytokines in abdominal aortic aneurysm: master regulators with clinical application. *Biomark Insights*. 2022;17:11772719221095676.
47. Liu CL, Ren J, Wang Y, et al. Adipocytes promote interleukin-18 binding to its receptors during abdominal aortic aneurysm formation in mice. *Eur Heart J*. 2020;41:2456–2468.
48. Davis FM, Rateri DL, Daugherty A. Abdominal aortic aneurysm: novel mechanisms and therapies. *Curr Opin Cardiol*. 2015;30:566–573.
49. Wilson WR, Anderton M, Choke EC, Dawson J, Loftus IM, Thompson MM. Elevated plasma MMP1 and MMP9 are associated with abdominal aortic aneurysm rupture. *Eur J Vasc Endovasc Surg*. 2008;35:580–584.
50. Hirose Y, Hamada S, Takamiya M, Imakita S, Naito H. [Growth rates of aortic aneurysms as a risk factor in rupture: an evaluation with CT]. *Nihon Igaku Hoshasen Gakkai Zasshi*. 1993;53:635–640.
51. Brewster DC, Cronenwett JL, Hallett JW Jr, et al. Guidelines for the treatment of abdominal aortic aneurysms. Report of a subcommittee of the Joint Council of the American Association for vascular surgery and Society for vascular surgery. *J Vasc Surg*. 2003;37:1106–1117.
52. Vorp DA. Biomechanics of abdominal aortic aneurysm. *J Biomech*. 2007;40:1887–1902.
53. Karthaus EG, Tong TML, Vahl A, Hamming JF, Dutch Society of Vascular Surgery tSCotDSAA, the Dutch Institute for Clinical A. Saccular abdominal aortic aneurysms: patient characteristics, clinical presentation, treatment, and outcomes in The Netherlands. *Ann Surg*. 2019;270:852–858.
54. Smith ME, Andraska EA, Sutzko DC, Boniakowski AM, Coleman DM, Osborne NH. The decline of open abdominal aortic aneurysm surgery among individual training programs and vascular surgery trainees. *J Vasc Surg*. 2020;71:1371–1377.

Submitted Apr 3, 2024; accepted Jun 8, 2024.

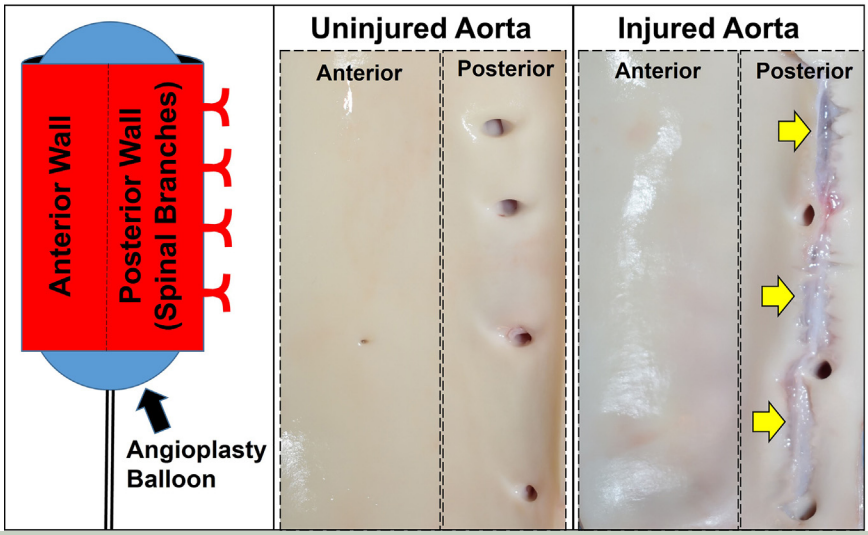

Supplementary Fig. After initial balloon angioplasty **(A)**, the aorta was opened along the side for comparison of anterior and posterior aortic wall. As compared with uninjured aorta **(B)**, the mechanical intimal injury consistently affects the posterior aortic wall **(C)**, an unfavorable area for enzymatic perfusion. (The posterior reveals openings to intercostal spinal cord branches.)

Supplementary Table. Comparisons of aneurysm models

Features	Mouse angiotensin II Infusion	Mouse open surgery enzyme	Porcine open surgery enzyme	Porcine dual balloon	Porcine xenogeneic patch	Porcine drug infusion stent graft
Index references	Daughtery et al[18]	Anidjar et al[15]	Eckhouse et al[24]; Shannon et al[25]	Lederman et al[21]	Perini et al[20]	Kenawy et al[26]
Absent xenogeneic confounders	✓	✓	✓	✓	x	✓
Hemodynamics similar to humans	x	x	✓	✓	✓	✓
Genotype independent	x	✓	?	?	?	?
Rapid surgical recovery	✓	x	x	✓	x	✓
Independent from hvoerlipidemia	x	✓	✓	✓	✓	✓
Absence of intra-abdominal scar	✓	x	x	✓	x	✓
Adequate length aneurysms	✓	✓	✓	x	✓	✓
Absence of distal ischemia	✓	x[a]	x	x	x	✓

[a]While original murine models detailed intraluminal infusion, subsequent reports have described periadventitial application of enzymes (Bhamidipati et al[16]) without compromise of distal perfusion.